Editors' Suggestion

Electric Auxetic Effect in Piezoelectrics

Jian Liu,[1,2,*] Shi Liu,[3,4,†] Jia-Yue Yang,[1,2] and Linhua Liu[1,2]
[1]*Optics and Thermal Radiation Research Center, Shandong University, Qingdao, Shandong 266237, China*
[2]*School of Energy and Power Engineering, Shandong University, Jinan, Shandong 250061, China*
[3]*School of Science, Westlake University, Hangzhou, Zhejiang 310024, China*
[4]*Institute of Natural Sciences, Westlake Institute for Advanced Study, Hangzhou, Zhejiang 310024, China*

(Received 4 May 2020; accepted 24 September 2020; published 2 November 2020)

Auxetic materials are characterized by a negative Poisson's ratio that they expand laterally in the directions perpendicular to the applied stretching stress and vice versa. Piezoelectrics will change their dimensions when exposed to an external electric field. Here we introduce the concept of the "electric auxetic effect": electric auxetic materials will contract or expand in all dimensions in response to an electric field. Such unusual piezoelectric response driven by an electric field is a close analogy to the auxetic effect driven by a stress field. A key feature of electric auxetic materials is that their longitudinal and transverse piezoelectric coefficients are of the same sign. We demonstrate using first-principles calculations that the $Pca2_1$ orthorhombic phase of ferroelectric HfO_2 exhibits both the negative longitudinal piezoelectric effect and the electric auxetic effect. The unusual negative longitudinal piezoelectric effect arises unexpectedly from the domination of the negative internal-strain contribution over the positive clamped-ion contribution, a character often found in van der Waals solids. We confirm a few more electric auxetic materials with finite electric field calculations by screening through a first-principles-based database of piezoelectrics.

DOI: 10.1103/PhysRevLett.125.197601

Auxetic materials [1,2] with a negative Poisson's ratio exhibit a counterintuitive structural response; i.e., they expand in the lateral direction when stretched longitudinally. Considerable efforts [3–5] have been made to discover and design auxetic materials for their potential applications, such as impact absorbers. Piezoelectrics is a class of functional materials that can change their dimensions in response to an electric field E. Piezoelectricity is described by the change of spontaneous polarization P_S in response to an applied strain ε ($\partial P_S/\partial\varepsilon$, piezoelectric stress coefficient e) or stress σ ($\partial P_S/\partial\sigma$, piezoelectric strain coefficient d) [6]. The two coefficients are related through $d_{ij} = e_{ik}S_{kj}$, where S is the elastic compliance constant. In experiments, the piezoelectric response is often characterized by d_{ij} through the direct piezoelectric effect $(\partial P_i/\partial\sigma_j)|_E$ or the converse piezoelectric effect $(\partial\varepsilon_j/\partial E_i)|_\sigma$. In first-principles calculations, it is often more convenient to discuss e_{ij} since its decomposition may provide fundamental physical insights. The piezoelectric effect is important in various applications, such as actuators [7] and nanogenerators [8,9].

Most piezoelectric materials exhibit positive (normal) longitudinal piezoelectricity ($d_{33} > 0$). To the best of our knowledge, the first discovered material possessing a negative d_{33} is the ferroelectric poly(vinylidene fluoride) (PVDF). It was observed in experiments that ferroelectric PVDF film becomes thinner upon the application of E along the poling direction [10,11]. This counterintuitive phenomenon, termed as the negative longitudinal piezoelectric effect (NLPE), was considered to be rare for a long time. The origin of the NLPE in ferroelectric PVDF is still a subject of debate, possibly due to the semicrystalline nature of this polymer [12–15]. Recent *in situ* dynamic x-ray diffraction measurements suggested that the negative d_{33} arises from the dynamics of the composite microstructure consisting of both crystalline and amorphous phases [16]. On the theory side, the NLPE was demonstrated for crystalline β-PVDF by various computational methods ranging from molecular dynamics simulations to first-principles calculations [17–19], suggesting its intrinsic origin. Single-phase materials exhibiting the NLPE have received revived attention in recent years. Following scattered first-principles predictions of negative e_{33} in some zinc blende (e.g., GaAs [20]) and wurtzite (e.g., BN [21,22]) piezoelectrics over the years, Liu and Cohen demonstrated the NLPE in several hexagonal *ABC* ferroelectrics and revealed that such negative response is a general phenomenon by screening through a computational database of piezoelectrics [23]. More recently, the NLPE was also discovered in van der Waals (vdW) layered solids such as $CuInP_2S_6$ [24] and bismuth tellurohalides BiTeX [25].

Here we introduce the concept of electric auxetic effect (analogous to the known auxetic effect): electric auxetic materials will contract or expand in all dimensions in response to an electric field. Here the deformation is driven by an electric field rather than a stress. In conventional piezoelectrics, the transverse (in the basal plane) and longitudinal (along the polar axis z) piezoelectric coefficients are generally of the opposite sign. For example, $PbTiO_3$ [26] has ($e_{31} < 0, e_{33} > 0$), whereas wurtzite BN [21] has ($e_{31} > 0$, $e_{33} < 0$). Consequently, with E in the direction of P_S, materials exhibiting positive (negative) longitudinal piezoelectricity would expand (contract) along the polar axis while they would contract (expand) in the lateral dimensions. We propose that there is no fundamental physics preventing the longitudinal and transverse piezoelectric coefficients having the same sign in a single-phase material. A piezoelectric with both negative (positive) e_{31} and e_{33} will contract (expand) in all dimensions in response to E applied in the direction of P_S. To the best of our knowledge, the electric auxetic effect has not been explored and this counterintuitive electric-field-driven structural response may offer novel avenues for the design of electromechanical devices.

Unexpected ferroelectricity (and hence piezoelectricity) was recently discovered in doped [27], undoped [28], and ZrO_2-alloyed [29] HfO_2 thin films. The origin of ferroelectricity in this conventional high-κ dielectric is commonly attributed to the $Pca2_1$ orthorhombic phase of HfO_2 (referred to as ferroelectric HfO_2 hereafter) that is stabilized by many extrinsic factors, such as dopants and residual stresses [27,30–36]. Because of its silicon compatibility, HfO_2-based piezoelectric thin film is a promising candidate for future piezoelectric devices at the nanoscale. Very recently, it was demonstrated by some of us, using first-principles calculations, that ferroelectric HfO_2 exhibits the NLPE [37], for which the underlying mechanism remains elusive.

In this Letter, using first-principles calculations, we demonstrate a significant NLPE in ferroelectric HfO_2 which persists upon ZrO_2 alloying and Si doping. The NLPE in HfO_2-based materials arises from the domination of the negative internal-strain contribution over the positive clamped-ion contribution. In addition to the NLPE, ferroelectric HfO_2 is an electric auxetic material exhibiting an overall contraction (expansion) with the application of E in (against) the direction of P_S. We further carried out data mining using a first-principles-based database of piezoelectrics and confirmed the electric auxetic effect in a few more vdW solids with finite electric field calculations. Notably, quasi-2D ternary compounds ASnX ($A =$ Na, K and $X = N$, P) crystallizing in the space group $P6_3mc$ are identified to be electric auxetic. The present Letter unravels and highlights the NLPE in the newly discovered ferroelectric HfO_2, which may have important implications for energy harvesting and sensor applications utilizing HfO_2-based piezoelectrics. Moreover, the electric auxetic effect is expected to open up new opportunities to control structural deformations using electric fields.

Density-functional theory calculations were carried out using the Quantum ESPRESSO (QE) package [38]. The spontaneous polarization is calculated using the modern theory of polarization (Berry-phase method) [20,39–41]. We use the Perdew-Zunger parametrization of the local density approximation (LDA) [42,43] and the Perdew-Burke-Ernzerhof (PBE) parametrization of the generalized gradient approximation [44] to describe the exchange-correlation functional for ferroelectric HfO_2 and $PbTiO_3$, respectively. Ultrasoft pseudopotentials are taken from the PSLibrary [45]. Maximally localized Wannier functions [46–48] are constructed using the Wannier90 [49,50] code interfaced with the QE package to obtain the locations of Wannier centers. Finite electric field calculations are performed using the method developed in Refs. [51–53], as implemented in the ABINIT package [54,55]. Piezoelectric stress and strain coefficients are calculated by density-functional perturbation theory [56]. All the structure figures are produced using VESTA [57]. More computational details can be found in the Supplemental Material [58].

We first study the piezoelectric properties of ferroelectric HfO_2. The e_{33} calculated using LDA is $-1.53\ \mathrm{C/m^2}$. In order to assess the performance of different functionals, PBE [44] and PBEsol [59] exchange-correlation functionals are employed, predicting the NLPE of similar magnitudes (-1.35 and $-1.44\ \mathrm{C/m^2}$, respectively). Such NLPE is even more significant than the most negative e_{33} found in NaZnSb ($-1.04\ \mathrm{C/m^2}$) among hexagonal ABC ferroelectrics [23]. Moreover, we find that the NLPE is robust upon ZrO_2 alloying and Si doping, since Hf, Zr, and Si ions carry similar Born effective charges (Z^*_{33}) of 4.98, 5.14, and 4.31 e, respectively, as shown in Fig. 1(a). Ferroelectric ZrO_2 possesses even larger NLPE than ferroelectric HfO_2, while their alloy ($Hf_xZr_{1-x}O_2$) exhibits a linear dependence of the NLPE on the composition x. The incorporation of Si dopants perturbs the local coordination environment of the host HfO_2 structure but has little impact on the lattice (and hence piezoelectricity).

It is of fundamental interest to understand the underlying mechanism responsible for the NLPE in ferroelectric HfO_2. Piezoelectricity is commonly decomposed into "clamped-ion" ($e^{(0)}_{33}$) and "internal-strain" ($e^{(i)}_{33}$) contributions [20,60]. The former describes the change of P_S due to a uniform distortion of the lattice, while the latter measures the piezoelectric response to atomic relaxations that release the internal strain. The decompositions are summarized in Table I for several NLPE materials, including β-PVDF, BiTeI, and NaZnSb (representative of 1D ferroelectric polymers, vdW layered BiTeX, and bulk hexagonal ABC ferroelectrics, respectively). In vdW layered materials such as $CuInP_2S_6$ [24] and BiTeX [25], due to the strong intralayer chemical bonds and the weak interlayer vdW interaction, the internal-strain contribution dominates as a result of large interlayer deformation. In ionic solids such as wurtzite BN [21,22] and hexagonal ABC

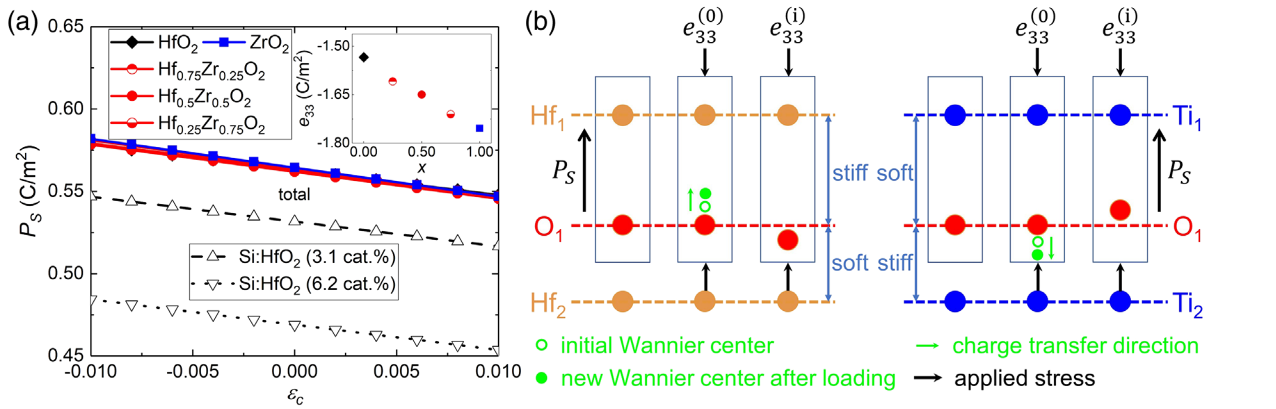

FIG. 1. (a) Spontaneous polarization P_S for HfO_2-based materials as a function of longitudinal strain ε_c. The slope corresponds to e_{33}. The inset shows the composition dependence of e_{33} for $Hf_{1-x}Zr_xO_2$. (b) Schematic illustration of the mechanism responsible for the NLPE in ferroelectric HfO_2, in comparison with conventional $PbTiO_3$. The unit cell (black box) is chosen such that the dipole formed by O_1 and $Hf_1(Ti_1)$ aligns with the bulk polarization, thus selecting the right polarization branch (quanta). The clamped-ion polarization scales with the dipole moment formed by the positive O_1 core (red circle) and the associated negative Wannier center (green circle). The "relaxed-ion" polarization scales with the dipole moment of $O_1-Hf_1(Ti_1)$. It is noted that in both ferroelectric HfO_2 and $PbTiO_3$, the Wannier center is in the "stiff" bond and O_1 atom moves into the "soft" region at the relaxed-strain state (see discussions in main text).

ferroelectrics [23], the clamped-ion contribution dominates because atomic relaxations are small due to the rigid potential energy surfaces.

In ferroelectric HfO_2-based materials, we find that the negative internal-strain contribution dominates over the positive clamped-ion contribution (see also Fig. S1 [58]). This is somewhat surprising since such tendency is often found in solids that condense through vdW interactions (such as β-PVDF and BiTeI, see Table I), whereas the large deviation of Z^*_{33} of Hf and O atoms from their nominal ionic charges suggests a mixed ionic-covalent character in ferroelectric HfO_2. Moreover, a direct comparison between HfO_2 and $PbTiO_3$ shows that their total, as well as individual decomposed longitudinal piezoelectricity, are all of the opposite sign, as shown in Table I.

We now offer a simple dipole model to explain the signs of $e^{(0)}_{33}$ and $e^{(i)}_{33}$ based on Wannier representations and Born effective charges, respectively, as schematically illustrated in Fig. 1(b) (see also the insets of Fig. 2 for structural models). The choice of the ferroelectric unit cell ensures the dipole moment aligning with the bulk polarization, thus selecting the correct polarization branch (quanta). The total polarization can be gauged by the dipole moment formed by the oppositely charged atoms carrying Born effective charges in the unit cell, while the effect of charge transfer is captured by the shift of Wannier centers. For simplicity, here we only focus on the displacement of O_1 atoms.

TABLE I. Calculated total, internal-strain, and clamped-ion piezoelectric stress coefficients (in units of C/m^2), compared with theoretical results from literatures (shown in parentheses) for $PbTiO_3$ [26], β-PVDF [19], BiTeI [25], and NaZnSb [23].

	e_{33}	$e^{(i)}_{33}$	$e^{(0)}_{33}$
HfO_2	−1.53	−2.16	0.63
$PbTiO_3$	2.55 (3.23)	3.49 (4.11)	−0.94 (−0.88)
β-PVDF	−0.34 (−0.33)	−0.49	0.15
BiTeI	−0.41 (−0.53)	−0.60 (−0.63)	0.19 (0.10)
NaZnSb	−1.23 (−1.04)	−0.25 (−0.09)	−0.98 (−0.95)

The pioneering work of Cohen [61] revealed that the ferroelectricity in perovskites such as $PbTiO_3$ arises from a delicate balance between the long-range Coulomb interaction (in favor of the ferroelectric phase) and the short-range repulsion (in favor of the paraelectric phase), while the latter is further weakened by the hybridization between Ti-d and O-p orbitals. As a result of the hybridization, the O_1 atom is associated with a Wannier center located at the *shorter* $Ti_2—O_1$ bond but closer to O_1 [see Fig. 1(b)]. Within the Wannier representation, the dipole formed by the positive O_1 core and the associated negative Wannier center is *parallel* to P_S. At the clamped-ion state, the $Ti_2—O_1$ bond becomes shorter as the lattice is compressed along the polar axis. A smaller distance between Ti_2 and O_1 strengthens both the repulsion and hybridization, but the repulsion becomes stronger than the hybridization [62]. This has two consequences. First, according to Harrison's bond-orbital model [63], the enhanced hybridization causes an effective charge transfer from the anion O_1 to the cation Ti_2, characterized by a downward shift of the Wannier center *against* the direction of P_S. This increases the distance between the O_1 core and the Wannier center, and hence the associated dipole moment as well as the polarization, resulting in the negative $e^{(0)}_{33}$ (enhanced polarization due to a compressive loading). Following that, the stronger repulsion will drive the elongation of the

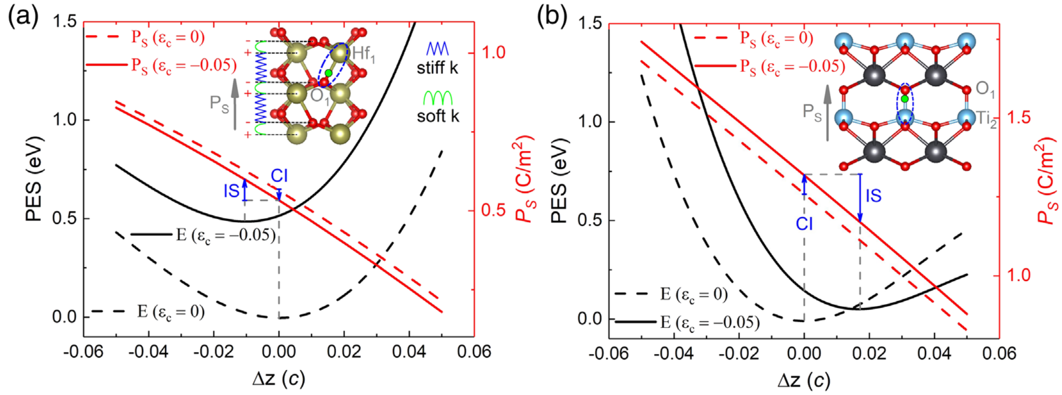

FIG. 2. Potential energy surfaces with the O_1 sublattice displaced along the polar axis (in fraction of lattice constant c) at the strain-free state (dashed lines) and the clamped-ion state with a compressive longitudinal strain of 5% (solid lines) for (a) ferroelectric HfO_2, (b) $PbTiO_3$. The bonds associated with the ferroelectric distortion are circled by dashed blue lines, with their Wannier centers schematically represented by green dots. The corresponding clamped-ion (CI) and internal-strain (IS) contributions are marked by blue arrows. For ferroelectric HfO_2, the ball-and-spring model is schematically illustrated. From anion to cation, "intralayer" ("interlayer") balls are linked by stiff (soft) springs in (against) the direction of P_S.

Ti_2—O_1 bond to the relaxed-ion state. This causes an upshift of the O_1 atom and a reduced dipole moment of Ti_1—O_1, and is hence responsible for the positive $e_{33}^{(i)}$.

From the above discussions, we are then ready to identify the structural origin of the NLPE in ferroelectric HfO_2. The ferroelectric distortion (from the nonpolar $P4_2/nmc$ tetragonal phase) involves not only longitudinal but also transverse displacement of the anion O_1 sublattice, with its coordination number varying from four to three. The total P_S is against the ferroelectric displacement of the O_1 sublattice. Although there are three Hf—O_1 bonds almost equal in length, the competition between hybridization and repulsion occurs mainly in one Hf_1—O_1 bond with the smallest zenith angle [circled by a dashed blue line in the inset of Fig. 2(a)]. More importantly, here the Wannier center associated with O_1 locates at the Hf_1—O_1 bond, and hence the corresponding dipole moment points against P_S. Consequently, at the clamped-ion state, the enhanced hybridization causes the Wannier center to shift toward the Hf_1 site; this reduces the total polarization and is hence responsible for the positive $e_{33}^{(0)}$. Similar to the case of $PbTiO_3$, in the relaxed-ion state, the repulsion will elongate the Hf_1—O_1 bond. The difference is that here O_1 moves *downward*, which naturally leads to the increased dipole moment of Hf_1—O_1 (enhanced polarization) and the negative $e_{33}^{(i)}$. As a result, the clamped-ion and internal-strain components are both of the opposite sign to that of $PbTiO_3$. Overall, the negative $e_{33}^{(i)}$ dominates over the positive $e_{33}^{(0)}$, giving rise to the NLPE in ferroelectric HfO_2.

First-principles calculations support our model discussed above. We calculate the potential energy surfaces (PESs) and the associated polarization by displacing the O_1 sublattice along the polar axis (Δz) in both strain-free ($\varepsilon_c = 0$) and compressed ($\varepsilon_c = -0.05$) states. The polarization at $\Delta z = 0$ for $\varepsilon_c = -0.05$ reflects the clamped-ion state polarization. As shown in Fig. 2 [see also Figs. S2(c) and S2(d) [58] for the displacements of the Wannier centers], it is evident that the strained ferroelectric HfO_2 ($PbTiO_3$) has a smaller (larger) polarization due to the upshift (downshift) of the O_1 Wannier center than that in the strain-free state at $\Delta z = 0$, indicating a positive (negative) $e_{33}^{(0)}$. The minimum of PES $(\Delta z)_{eq}$ corresponds to the equilibrium relaxed-ion state for a given strain. We find that ferroelectric HfO_2 ($PbTiO_3$) has $(\Delta z)_{eq} < 0\,(> 0)$ at $\varepsilon_c = -0.05$, corresponding to a downward (upward) shift of O_1 and increased Hf_1—O_1 (Ti_2—O_1) bond length, and the polarization is larger (smaller) than that at $(\Delta z)_{eq} = 0$ in the strain-free state, indicating a negative (positive) $e_{33}^{(i)}$ and e_{33}. Simply put, the key structural difference between $PbTiO_3$ and ferroelectric HfO_2 is that the "stiffer" bond (long Hf_1—O_1 bond and short Ti_2—O_1 bond, see the slopes of PESs in Fig. 2) have opposite cation-anion orientations with respect to the bulk polarization. Following the ball-and-spring model [24] (the cation and anion sublattices are treated as atomic planes of effective charges alternating in the polar direction), the PES of ferroelectric HfO_2 exhibits a remarkable similarity to those of vdW solids [see Fig. 2(a) for schematic illustrations], and hence the negative internal-strain contribution dominates over the positive clamped-ion contribution.

In most conventional ferroelectrics such as $PbTiO_3$ [26] and nonferroelectrics such as wurtzite semiconductors [20], the transverse and longitudinal piezoelectric coefficients are negative and positive respectively ($e_{31} < 0$, $e_{33} > 0$); i.e., these materials exhibit "normal" piezoelectric effect. Materials exhibiting the NLPE, however, are not necessarily electric auxetic materials (e.g., wurtzite BN [21,22] has $e_{31} > 0$, $e_{33} < 0$). One exception is the case of β-

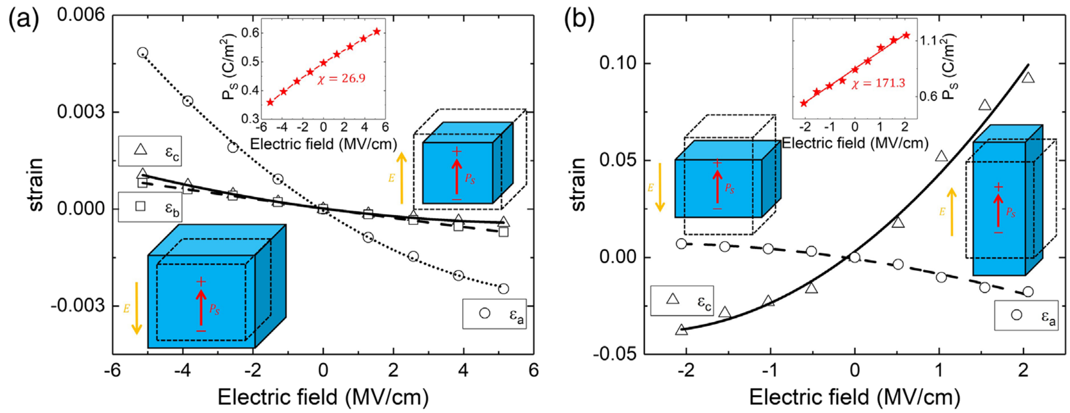

FIG. 3. Spontaneous polarization P_S and strain in response to an applied electric field E for (a) ferroelectric HfO_2, (b) $PbTiO_3$. The slope of the P_S-E curve gives the electric susceptibility χ. The insets show schematically the converse piezoelectric response.

PVDF, whose e_{ij} are all negative [19]. Interestingly, we find that ferroelectric HfO_2 is also an electric auxetic material. The calculated proper d_{31}, d_{32}, and d_{33} are −1.25, −1.84, and −2.59 pm/V, respectively. To further demonstrate the electric auxetic effect, we perform first-principles calculations at finite E where the lattice and the atomic positions are fully relaxed. As expected, within the experimentally relevant E values ($|E| < 5$ MV/cm), ferroelectric HfO_2 indeed exhibits electric auxeticity, as shown in Fig. 3(a). For comparison, we also demonstrate the normal converse piezoelectric response in $PbTiO_3$ ($d_{31} < 0$, $d_{33} > 0$), as shown in Fig. 3(b).

We then search for electric auxetic materials among other materials exhibiting the NLPE, as shown in Fig. 4 and Table SI [58]. We find that vdW solids such as β-PVDF and BiTeI are generally electric auxetic. The ionic solid NaZnSb, on the other hand, exhibits the NLPE but is not electric auxetic ($d_{31} > 0$, $d_{33} < 0$). We further carried out data mining using a first-principles-based database of piezoelectrics [64] and identified over 100 compounds with

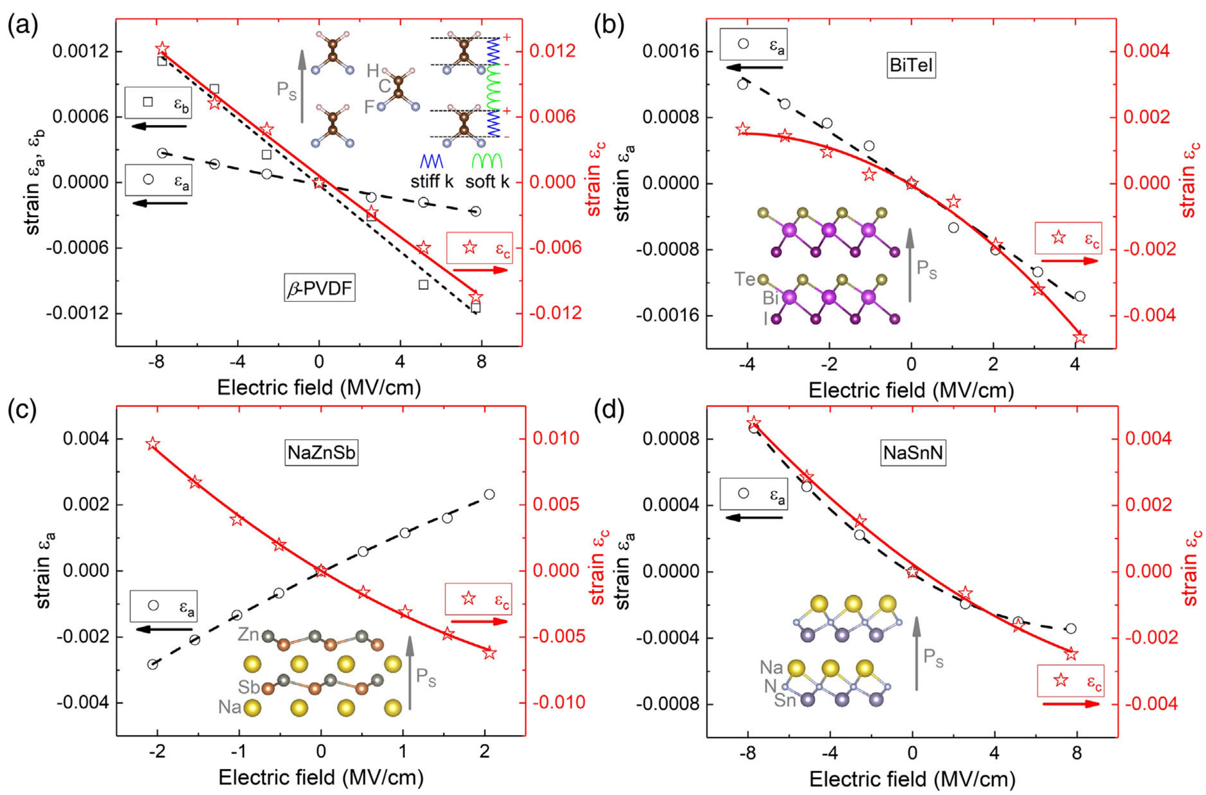

FIG. 4. Strain in response to an applied electric field E for (a) β-PVDF, (b) BiTeI, (c) NaZnSb, and (d) NaSnN. The ball-and-spring model for β-PVDF resembles its similarity to ferroelectric HfO_2 in their structures.

either all positive or all negative e_{3i} (see Supplemental Material [58]). Notably, quasi-2D ternary compounds ASnX (A = Na, K and X = N, P) crystallizing in the space group $P6_3mc$ have all negative e_{31} (d_{31}) and e_{33} (d_{33}), as shown in Table SII [58]. The mechanism of the NLPE in these materials is similar to other vdW solids; i.e., the negative internal-strain contribution dominates. Their electric auxetic behaviors are confirmed with finite electric field calculations for the case of NaSnN [see Fig. 4(d)]. All in all, our preliminary results suggest that electric auxeticity might be a general feature for vdW solids exhibiting the NLPE.

In summary, we have demonstrated a significant NLPE in ferroelectric HfO_2-based materials with first-principles calculations. An unexpected similarity between ferroelectric HfO_2 and vdW solids is found in the underlying mechanism responsible for the unusual NLPE: the negative internal-strain contribution dominates over the positive clamped-ion contribution. Applying an electric field along (against) the spontaneous polarization of ferroelectric HfO_2 and several other vdW solids results in an overall contraction (expansion) of the lattice, confirming the electric auxetic effect. The results of data mining reveal over 100 compounds with significant electric auxetic effect. We hope that this Letter will stimulate future theoretical and experimental studies of the NLPE and the electric auxetic effect, which may have important implications for energy harvesting and sensor applications.

J. L. was supported by the Qilu Young Scholar Program of Shandong University. J. L. acknowledges the support from the National Natural Science Foundation of China (Grant No. 11904202). S. L. was supported by foundation of Westlake University and acknowledges the computational resource provided by Supercomputer Center at Westlake University.

[*]Jian.Y.Liu@sdu.edu.cn
[†]liushi@westlake.edu.cn

[1] R. Lakes, Science **235**, 1038 (1987).
[2] K. E. Evans and A. Alderson, Adv. Mater. **12**, 617 (2000).
[3] J. Dagdelen, J. Montoya, M. de Jong, and K. Persson, Nat. Commun. **8**, 323 (2017).
[4] R. Peng, Y. Ma, Z. He, B. Huang, L. Kou, and Y. Dai, Nano Lett. **19**, 1227 (2019).
[5] R. Peng, Y. Ma, Q. Wu, B. Huang, and Y. Dai, Nanoscale **11**, 11413 (2019).
[6] D. Damjanovic, Rep. Prog. Phys. **61**, 1267 (1998).
[7] K. Uchino, *Piezoelectric Actuators and Ultrasonic Motors* (Kluwer Academic, Boston, 1996).
[8] Z. L. Wang and J. Song, Science **312**, 242 (2006).
[9] X. Wang, J. Song, J. Liu, and Z. L. Wang, Science **316**, 102 (2007).
[10] H. Burkard and G. Pfister, J. Appl. Phys. **45**, 3360 (1974).
[11] H. Ohigashi, J. Appl. Phys. **47**, 949 (1976).
[12] Y. Wada and R. Hayakawa, Jpn. J. Appl. Phys. **15**, 2041 (1976).
[13] R. Kepler and R. Anderson, J. Appl. Phys. **49**, 4490 (1978).
[14] T. Furukawa, IEEE Trans. Electr. Insul. **24**, 375 (1989).
[15] T. Furukawa and N. Seo, Jpn. J. Appl. Phys. **29**, 675 (1990).
[16] I. Katsouras, K. Asadi, M. Li, T. B. Van Driel, K. S. Kjaer, D. Zhao, T. Lenz, Y. Gu, P. W. Blom, and D. Damjanovic, Nat. Mater. **15**, 78 (2016).
[17] K. Tashiro, M. Kobayashi, H. Tadokoro, and E. Fukada, Macromolecules **13**, 691 (1980).
[18] J. D. Carbeck and G. C. Rutledge, Polymer **37**, 5089 (1996).
[19] S. M. Nakhmanson, M. B. Nardelli, and J. Bernholc, Phys. Rev. Lett. **92**, 115504 (2004).
[20] F. Bernardini, V. Fiorentini, and D. Vanderbilt, Phys. Rev. B **56**, R10024 (1997).
[21] K. Shimada, Jpn. J. Appl. Phys. **45**, L358 (2006).
[22] K. Shimada, T. Sota, K. Suzuki, and H. Okumura, Jpn. J. Appl. Phys. **37**, L1421 (1998).
[23] S. Liu and R. Cohen, Phys. Rev. Lett. **119**, 207601 (2017).
[24] L. You, Y. Zhang, S. Zhou, A. Chaturvedi, S. A. Morris, F. Liu, L. Chang, D. Ichinose, H. Funakubo, and W. Hu, Sci. Adv. **5**, eaav3780 (2019).
[25] J. Kim, K. M. Rabe, and D. Vanderbilt, Phys. Rev. B **100**, 104115 (2019).
[26] G. Sághi-Szabó, R. E. Cohen, and H. Krakauer, Phys. Rev. Lett. **80**, 4321 (1998).
[27] T. Böscke, J. Müller, D. Bräuhaus, U. Schröder, and U. Böttger, Appl. Phys. Lett. **99**, 102903 (2011).
[28] P. Polakowski and J. Müller, Appl. Phys. Lett. **106**, 232905 (2015).
[29] J. Müller, T. Böscke, D. Bräuhaus, U. Schröder, U. Böttger, J. Sundqvist, P. Kücher, T. Mikolajick, and L. Frey, Appl. Phys. Lett. **99**, 112901 (2011).
[30] J. Müller, T. S. Böscke, U. Schröder, S. Mueller, D. Bräuhaus, U. Böttger, L. Frey, and T. Mikolajick, Nano Lett. **12**, 4318 (2012).
[31] R. Batra, T. D. Huan, J. L. Jones, G. Rossetti, Jr., and R. Ramprasad, J. Phys. Chem. C **121**, 4139 (2017).
[32] M. H. Park, T. Schenk, C. M. Fancher, E. D. Grimley, C. Zhou, C. Richter, J. M. LeBeau, J. L. Jones, T. Mikolajick, and U. Schroeder, J. Mater. Chem. C **5**, 4677 (2017).
[33] S. Clima, D. Wouters, C. Adelmann, T. Schenk, U. Schroeder, M. Jurczak, and G. Pourtois, Appl. Phys. Lett. **104**, 092906 (2014).
[34] X. Sang, E. D. Grimley, T. Schenk, U. Schroeder, and J. M. LeBeau, Appl. Phys. Lett. **106**, 162905 (2015).
[35] R. Materlik, C. Künneth, and A. Kersch, J. Appl. Phys. **117**, 134109 (2015).
[36] T. D. Huan, V. Sharma, G. A. Rossetti, Jr., and R. Ramprasad, Phys. Rev. B **90**, 064111 (2014).
[37] J. Liu, S. Liu, L. Liu, B. Hanrahan, and S. Pantelides, Phys. Rev. Applied **12**, 034032 (2019).
[38] P. Giannozzi *et al.*, J. Phys. Condens. Matter **21**, 395502 (2009).
[39] R. King-Smith and D. Vanderbilt, Phys. Rev. B **47**, 1651 (1993).
[40] R. Resta and D. Vanderbilt, Theory of polarization: A modern approach, in *Physics of Ferroelectrics. Topics in*

Applied Physics (Springer, Berlin, Heidelberg, 2007), Vol. 105, pp. 31–68, https://doi.org/10.1007/978-3-540-34591-6_2.
[41] R. Resta, M. Posternak, and A. Baldereschi, Phys. Rev. Lett. **70**, 1010 (1993).
[42] D. M. Ceperley and B. Alder, Phys. Rev. Lett. **45**, 566 (1980).
[43] J. P. Perdew and A. Zunger, Phys. Rev. B **23**, 5048 (1981).
[44] J. P. Perdew, K. Burke, and M. Ernzerhof, Phys. Rev. Lett. **77**, 3865 (1996).
[45] A. Dal Corso, Comput. Mater. Sci. **95**, 337 (2014).
[46] N. Marzari and D. Vanderbilt, Phys. Rev. B **56**, 12847 (1997).
[47] I. Souza, N. Marzari, and D. Vanderbilt, Phys. Rev. B **65**, 035109 (2001).
[48] N. Marzari, A. A. Mostofi, J. R. Yates, I. Souza, and D. Vanderbilt, Rev. Mod. Phys. **84**, 1419 (2012).
[49] A. A. Mostofi, J. R. Yates, Y.-S. Lee, I. Souza, D. Vanderbilt, and N. Marzari, Comput. Phys. Commun. **178**, 685 (2008).
[50] A. A. Mostofi, J. R. Yates, G. Pizzi, Y.-S. Lee, I. Souza, D. Vanderbilt, and N. Marzari, Comput. Phys. Commun. **185**, 2309 (2014).
[51] I. Souza, J. Íñiguez, and D. Vanderbilt, Phys. Rev. Lett. **89**, 117602 (2002).
[52] R. Nunes and X. Gonze, Phys. Rev. B **63**, 155107 (2001).
[53] P. Umari and A. Pasquarello, Phys. Rev. Lett. **89**, 157602 (2002).
[54] X. Gonze, B. Amadon, P.-M. Anglade, J.-M. Beuken, F. Bottin, P. Boulanger, F. Bruneval, D. Caliste, R. Caracas, and M. Côté, Comput. Phys. Commun. **180**, 2582 (2009).
[55] X. Gonze, F. Jollet, F. A. Araujo, D. Adams, B. Amadon, T. Applencourt, C. Audouze, J.-M. Beuken, J. Bieder, and A. Bokhanchuk, Comput. Phys. Commun. **205**, 106 (2016).
[56] X. Gonze and C. Lee, Phys. Rev. B **55**, 10355 (1997).
[57] K. Momma and F. Izumi, J. Appl. Crystallogr. **44**, 1272 (2011).
[58] See Supplemental Material at http://link.aps.org/supplemental/10.1103/PhysRevLett.125.197601 for further descriptions of computational setups.
[59] J. P. Perdew, A. Ruzsinszky, G. I. Csonka, O. A. Vydrov, G. E. Scuseria, L. A. Constantin, X. Zhou, and K. Burke, Phys. Rev. Lett. **100**, 136406 (2008).
[60] A. Dal Corso, M. Posternak, R. Resta, and A. Baldereschi, Phys. Rev. B **50**, 10715 (1994).
[61] R. E. Cohen, Nature (London) **358**, 136 (1992).
[62] Z. Wu and R. E. Cohen, Phys. Rev. Lett. **95**, 037601 (2005).
[63] W. A. Harrison, *Electronic Structure and the Properties of Solids* (W. H. Freeman and Company, San Francisco, 1980).
[64] M. De Jong, W. Chen, H. Geerlings, M. Asta, and K. A. Persson, Sci. Data **2**, 150053 (2015).